

# Revisiting the constraints on primordial black hole abundance with the isotropic gamma ray background

Siyu Chen,<sup>1</sup> Hong-Hao Zhang,<sup>1,\*</sup> and Guangbo Long<sup>1,†</sup>

<sup>1</sup>*School of Physics, Sun Yat-sen University, Guangzhou, Guangdong, People's Republic of China*

We revisit the constraints on primordial black holes (PBHs) in the mass range  $10^{13} - 10^{18}$  g by comparing the 100 keV-5 GeV gamma-ray background with isotropic flux from PBH Hawking radiation (HR). We investigate three effects that may update the constraints on the PBH abundance; i) reliably calculating the secondary spectra of HR for energy below 5 GeV, ii) the contributions to the measured isotropic flux from the Galactic PBH HR and that from annihilation radiation due to evaporated positrons, iii) inclusion of astrophysical background from gamma-ray sources. The conservative constraint is significantly improved by more than an order of magnitude at  $2 \times 10^{16}$  g  $\lesssim M \lesssim 10^{17}$  g over the past relevant work, where the effect ii is dominant. After further accounting for the astrophysical background, more than a tenfold improvement extends to a much wider mass range  $10^{15}$  g  $\lesssim M \lesssim 2 \times 10^{17}$  g.

## I. INTRODUCTION

Primordial black holes (PBHs) are the only candidate that can solve the dark matter (DM) problem without involving new physics [1, 2]. At present, there are still open PBH mass windows (e.g.,  $10^{17}$ - $10^{22}$  g) that can constitute all or most of the DM all over the universe, see e.g., [1]. If the PBHs contribute significantly to the DM, then the time-integrated Hawking radiation (HR) of PBHs with a mass of about  $10^{13}$ - $10^{18}$  g should significantly affect on the observed isotropic diffuse gamma-ray background (IGRB) and/or cosmic X-ray background (CXB) for energy above 100 keV [1, 3–7]. In order for HR to propagate through the intergalactic medium, these PBHs must survive at least into the transparent age of the cosmic microwave background (CMB) [4]. This condition sets the above PBH mass lower limit. In addition, the energy at the peak of HR decreases with increasing PBH mass. The contribution from PBHs larger than  $10^{18}$  g is concentrated in CXB below 100 keV, but is negligible [4].

Carr *et al.* [3] limited the PBH abundance conservatively within about  $10^{13}$ - $10^{18}$  g based on the evaporated contribution of PBHs that did not exceed the observed extragalactic photon background in the 100 keV-100 GeV range. Recently, Arber *et al.* [4] and Carr *et al.* [8] updated the bound with updated background observations (new Fermi-LAT data), and the former [4] also studied extended mass functions of Kerr black holes. Balles-teros *et al.* [5] and Iguaz *et al.* [6] set tighter bound in the mass range  $10^{16}$ - $10^{18}$  g with hard CXB and soft IGRB taking into account the emission from AGNs (Active galactic nucleus), respectively. It is worth emphasizing that [6] considers the contribution of the Galactic PBH emission and the annihilation radiation due to evapo-

rated positrons to the measured isotropic flux.

In addition to the above constraints using the isotropic cosmic photon background, there are many other limits on PBHs in the mass range  $5 \times 10^{14}$ - $10^{18}$  g based on the inconsistency between predicted HR-induced signatures and actual observations. These observations can be electron or positron cosmic rays [13], the cosmic microwave background [10–12], gamma-rays and X-ray fluxes from specific objects [14–17], neutrinos [18, 19], and so on. Their resulting excluded region of PBH mass and abundance are about similar to those from the cosmic photon background.

In this work, we aim to improve the constraints on the PBH abundance by comparing the simulated isotropic flux of PBHs and astrophysical sources with the observed IGRB in the **0.1 MeV-5 GeV** range<sup>1</sup>. Compared with past relevant works, in particular Ref. [4], three improvements on the treatments of the isotropic flux that may eventually improve the constraints will be investigated: (i) The IGRB from unresolved sources, such as AGNs and SFGs (star-forming galaxies), is modeled according to [25] and [26]. (ii) We reliably model the secondary spectrum of PBH HR below 5 GeV with the latest public code `BlackHawk`. 2.0 [28], which calculates the final state radiation (FSR) and decays of PBHs's primary particles (leptons and pions) below 5 GeV as discussed in [20]. (iii) We extend the analysis of Ref. [6] from the observed 10 keV-10 MeV flux to our 100 keV-5 GeV one. We take into account the diffuse flux contributed by the Galactic, which is measured by the detectors but cannot be separated from the truly extragalactic contribution, and an indirect component by the  $e^{\pm}$  annihilation via a positronium generated by the charge exchange between atomic hydrogen and positron evaporated from PBHs [6].

\* Corresponding author. [zh98@mail.sysu.edu.cn](mailto:zh98@mail.sysu.edu.cn)

† Corresponding author. [longgb@mail2.sysu.edu.cn](mailto:longgb@mail2.sysu.edu.cn)

<sup>1</sup> In general, IGRB is referred as observations of [48] and [50]. For convenience, all data used in this paper is broadly referred to as IGRB.

The plan of this paper is as follows. In Sec. II and III, we provide computational details of the isotropic flux from PBH HR, illustrate the data sets of cosmic background spectrum, and describe the models for the astrophysical background. Then, in Sec. IV we analyze the data and give our new constraints on the PBHs abundance. Finally, discussions and conclusions are presented in Sec. V and VI.

## II. HAWKING RADIATION FROM PBHS

### A. Hawking radiation from single PBH

In this work, we assume the mass distribution of PBHs is monochromatic and let us denote  $E$  as the photon energy in the local cosmic frame. The total photon spectrum  $\frac{d\dot{N}}{dE}$  emitted by a single PBH with mass  $M$ , in unit energy and unit time, can be written as (see e.g., [3])

$$\frac{d\dot{N}}{dE} = \frac{d\dot{N}^{\text{pri}}}{dE} + \frac{d\dot{N}^{\text{sec}}}{dE}. \quad (1)$$

The primary component  $\frac{d\dot{N}^{\text{pri}}}{dE}$  results from the direct Hawking emission, which is similar to the blackbody radiation but with a greybody factor counting the probability that a Hawking particle evades the PBH gravitational well. The secondary component (the second term) comes from the decay of the hadrons produced by the fragmentation of primary quarks and gluons.

In recent years, the HR spectra  $\frac{d\dot{N}}{dE}$  are usually calculated with the popular public code `BlackHawk. 1`, e.g., [4–6]. However, for the primary particles with energy below 5 GeV, it uses “extrapolation tables” to compute the secondary spectra, and thus these spectra are unreliable [20]. Thanks to Coogan *et al.*’s work [20], the latest version of this code (`BlackHawk. 2.0` [28]) incorporating the method of [20] can reliably simulate the secondary spectra from the FSR and the decay of the primary particles. This method takes advantage of the Altarelli-Parisi splitting functions to model the FSR and uses new `Hazma` to compute the photon spectrum from decays by [20]:

$$\begin{aligned} \frac{d\dot{N}^{\text{sec}}}{dE} &= \sum_{i=e^{\pm}, \mu^{\pm}, \pi^{\pm}} \int dE_i \frac{d\dot{N}_i^{\text{pri}}}{dE_i} \frac{dN_i^{\text{FSR}}}{dE} \\ &+ \sum_{i=\mu^{\pm}, \pi^0, \pi^{\pm}} \int dE_i \frac{d\dot{N}_i^{\text{pri}}}{dE_i} \frac{dN_i^{\text{decay}}}{dE}, \end{aligned} \quad (2)$$

where  $\frac{d\dot{N}_i^{\text{pri}}}{dE_i}$  are the primary spectra of leptons and pions. The explicit expression of  $\frac{dN_i^{\text{decay}}}{dE}$  and the FSR spectra  $\frac{dN_i^{\text{FSR}}}{dE}$  can be seen in [9] and [20], respectively.

As an improvement over the past relevant works [4–6], we simulate the secondary photon spectrum and the primary spectra of all particles with `BlackHawk. 2.0` [28]. Fig. 1 shows the resulting low energy correction in

the secondary spectrum. For small PBH mass range, e.g.,  $M = 10^{15}$  g, the new method (the blue line in Fig. 1) gives higher flux in the lower energy band than `BlackHawk. 1`. For large mass, e.g.,  $M = 3.5 \times 10^{16}$  g, it first gives weaker flux and then turns to higher in the lower energy band.

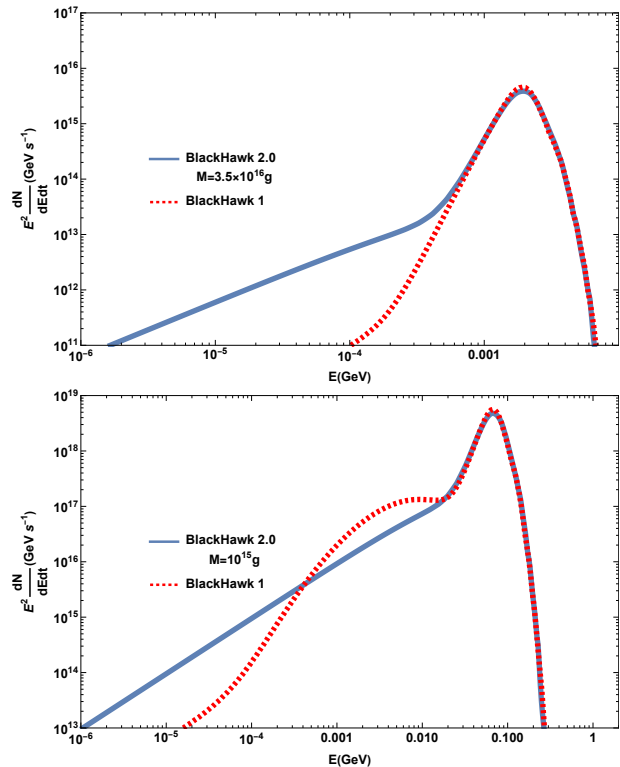


FIG. 1. The secondary spectra for  $M = 3.5 \times 10^{16}$  g (top) and  $M = 10^{15}$  g (bottom) obtained by different version of `BlackHawk`. The solid line represents that the spectrum is calculated with Eq. (2) using `BlackHawk. 2.0` [28] and the dash line represents one from `BlackHawk. 1.2` [24].

### B. The flux from extragalactic and Galactic PBHs

We consider the total diffuse flux emitted by PBHs throughout the universe. The flux can be separated to an extragalactic and Galactic part as

$$\frac{dN}{dE} = \frac{dN_{\text{EG}}}{dE} + \frac{dN_{\text{Gal}}}{dE}. \quad (3)$$

Each part includes a direct photon component and an indirect one from  $e^+$  annihilations [6], corresponding to the photon spectrum  $\frac{d\dot{N}}{dE}$  and  $\frac{d\dot{N}^{\text{ann.}}}{dE}$  from a single PBH respectively.

The measured extragalactic flux from a population of extragalactic PBHs of mass  $M$  with different ages is the

redshifted sum over all epoch emissions [3, 4]

$$\frac{dN_{\text{EG}}}{dE} \approx \frac{c}{4\pi} n_{\text{PBH}}(t_0) \int_{t_{\text{min}}}^{\min(t_0, \tau)} dt (1+z(t)) \quad (4)$$

$$\left( \frac{d\dot{N}_{\text{EG}}}{dE} (M(t), (1+z(t))E) + \frac{d\dot{N}_{\text{EG}}^{\text{ann.}}}{dE} (M(t), (1+z(t))E) \right),$$

where  $M(t)$  is a time dependent mass of a PBH,  $z(t) = (H_0 t)^{-2/3} - 1$  is the redshift parameter with the Hubble constant  $H_0$ , and  $n_{\text{PBH}}(t_0) \approx \frac{f\rho}{M}$  represents the number density of PBHs for a given initial mass  $M$  at the present universe's age  $t_0$ . Factor  $f = \Omega_{\text{PBH}}/\Omega_{\text{DM}}$  is a fraction of the total DM density in the Universe, and  $\rho = 2.17 \times 10^{-30} \text{ g cm}^{-3}$  denotes the current DM density of the Universe [29]. The integration runs from the time at last scattering of the CMB  $t_{\text{min}} = 380\,000$  years to  $t_{\text{max}} = \text{Max}(\tau(M), t_0)$  where  $\tau(M) \propto M^3$  is the lifetime of PBHs.

We assume the positrons emitted in the PBH evaporation can form positronium (Ps) with electrons of atoms in cosmological medium, following Ref. [6]. Since the case of  $e^\pm$  annihilation via Ps formation ( $f_{\text{Ps}}=1$ ) is more realistic than the direct  $e^\pm$  annihilation ( $f_{\text{Ps}}=0$ ), we only consider the former [30]. An annihilation of para-positronium can yield two photons and an ortho-positronium one yields three, with a total energy of  $2m_e c^2$  [31]. Thus, the indirect photon component in Eq. (4) can be written as

$$\frac{dN_{\text{EG}}^{\text{ann.}}}{dE} = \frac{c}{4\pi} n_{\text{PBH}}(t_0) \left( \dot{N}_{e^+}(M(t_c)) \cdot 2 \times \frac{1}{4} \frac{m_e c^2}{E} \delta[m_e c^2 - E(1+z(t_c))] + 3 \times \frac{3}{4} \int_{t_{\text{min}}}^{t_{\text{max}}} dt (1+z) \dot{N}_{e^+}(M(t)) \frac{1}{N_{3\gamma}} \frac{dN_{3\gamma}}{d[(1+z)E]} \right), \quad (5)$$

where  $\dot{N}_{e^+} = \int dE' \frac{d\dot{N}_{e^+}}{dE'}$  is the number of  $e^+$  emitted by a PBH in unit time [6] and  $\dot{N}_{e^+}(M(t_c))$  represents the  $e^+$  number at  $t_c$ , where  $t_c$  satisfies the equation  $E(1+z(t_c)) = m_e c^2$  and inequation  $t_{\text{min}} \leq t_c \leq t_{\text{max}}$ . The factors  $\frac{1}{4}$  and  $\frac{3}{4}$  describe the rate of the emitted photons in para-positronium and ortho-positronium state, respectively [31]. The energy spectrum of para-positronium annihilation is described by the Heaviside step-function  $\theta$  (it should be Dirac function if the photons are not redshifted). The normalized spectrum of ortho-positronium annihilation is denoted by [32]

$$\frac{1}{N_{3\gamma}} \frac{dN_{3\gamma}}{d[(1+z)E]} = \frac{2}{(1+z)(\pi^2 - 9)m_e c^2} \left( \frac{1-x}{x(\frac{2}{x} - 1)^2} + \frac{2(1-x)}{x^2} \ln(1-x) - \frac{2(1-x)^2}{(2-x)^3} \ln(1-x) + \frac{2}{x} - 1 \right), \quad (6)$$

where  $x = E/m_e c^2$  and the relation  $\frac{1}{N_{3\gamma}} \frac{dN_{3\gamma}}{d[(1+z)E]} d[(1+z)E] = \frac{1}{N_{3\gamma}} \frac{dN_{3\gamma}}{dE} dE$  has been used.

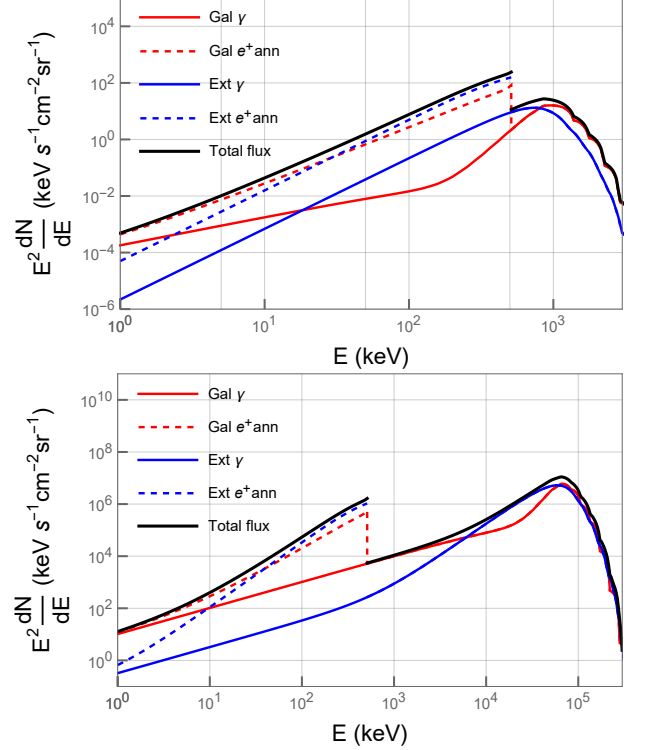


FIG. 2. Different parts of the total diffuse flux in Eq. (3) for  $M = 7 \times 10^{16} \text{ g}$ ,  $f = 1$  (top panel) and  $M = 10^{15} \text{ g}$ ,  $f = 1$  (bottom panel): the direct Galactic and extragalactic contributions, and their indirect  $e^+$  annihilation ones.

Since we are embedded inside the Galactic halo, an diffuse flux from the Galactic PBHs cannot be separated into the truly extragalactic contribution when the flux is measured by detectors; see [6] for details. Therefore, it should be taken into account in our simulation. As this flux depends on the integral along the line of sight of the Galactic DM distribution, and a conservative estimation of it is given by [6]

$$\frac{dN_{\text{Gal}}}{dE} = \frac{f}{4\pi M} \mathcal{D}_{\text{min}} \left( \frac{d\dot{N}_{\text{Gal}}}{dE} + \frac{d\dot{N}_{\text{Gal}}^{\text{ann.}}}{dE} \right), \quad (7)$$

where  $\mathcal{D}_{\text{min}}$  is the minimum of  $D$ -factor:

$$\mathcal{D}_{\text{min}} \equiv \int_{\text{GAC}} ds \rho_g, \quad (8)$$

where GAC denotes the line of sight towards the Galactic anti-center, namely  $l = 180^\circ$  and  $b = 0^\circ$  in galactic coordinates, and  $\rho_g$  is the DM distribution assumed a Navarro-Frenk-White profile with parameters  $r_s = 9.98 \text{ kpc}$ ,  $\rho_s = 2.2 \times 10^{-24} \text{ g cm}^{-3}$  [33].

The photon spectrum of positronium annihilation is

$$\frac{d\dot{N}_{\text{Gal}}^{\text{ann.}}}{dE} = \dot{N}_{e^+} \left( 2 \times \frac{1}{4} \delta(m_e c^2 - E) + 3 \times \frac{3}{4} \frac{1}{N_{3\gamma}} \frac{dN_{3\gamma}}{dE} \right), \quad (9)$$

where  $\frac{1}{N_{3\gamma}} \frac{dN_{3\gamma}}{dE}$  is defined by Eq. (6) letting  $z = 0$ .

We calculate the photon and positron spectra from a single PBH with `BlackHawk.2.0` [28]. Fig. 2 shows the contributions from the Galactic and extragalactic direct/indirect components to the total simulated IGRB flux in Eq. (3), for  $M = 7 \times 10^{16} \text{g}$ ,  $f = 1$  (top panel) and  $M = 10^{15} \text{g}$ ,  $f = 1$  (bottom panel) independently. As one can see, the flux (red line) from the Galactic direct HR can be several times larger than the extragalactic one (blue line) at around the peak of the spectrum, especially for massive PBHs. The component from the  $e^+$  annihilation can be larger than direct one, which would play an important role in contributing to the 100-511 keV IGRB.

### III. DATASETS AND THE ASTROPHYSICAL BACKGROUND MODELING

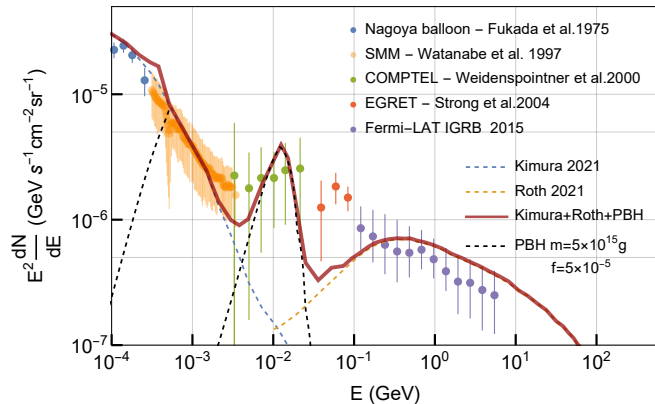


FIG. 3. The IGRB spectrum as measured by Fermi-LAT [48], EGRET [50], COMPTEL [49], SMM [47] and Nagoya balloon missions [52]. The Fermi-LAT data corresponds to the foreground model C [48], and the Galactic-foreground modeling uncertainty is added in quadrature to the data with  $1\sigma$  stochastic error. Kimura model [27] (blue dashed line) represents the contribution of low-luminosity AGN to the IGRB flux, Roth model [25] (red dashed line) represents the contribution from star-forming galaxies (SFG), and the PBHs’s contribution is represented with dashed black line. The sum of the three models is also shown with the red line.

The IGRB is the measured gamma-ray emission including all unresolved extragalactic emissions in a given survey and any residual (approximate) isotropic Galactic foregrounds [48]. In this study, we use the observed IGRB of HEAO-1+balloon, SMM, COMPTEL, EGRET and Fermi-LAT (foreground model C) from 100 keV to 5 GeV <sup>2</sup> as shown in Fig. 3, which corresponds to the

<sup>2</sup> In general, IGRB is referred to as observations of [48] and [50]. For convenience, all data used in this paper is broadly referred to as IGRB.

region where the PBH HR in the mass range  $10^{13} \text{g}$ - $10^{18} \text{g}$  is expected to contribute to the IGRB significantly. The Fermi-LAT data with energy  $\gtrsim 6 \text{GeV}$  is not chosen because of the two following facts. The background above GeV is expected to be mainly contributed by the  $10^{14}$ - $10^{15} \text{g}$  PBHs [3]. Though the HR of  $10^{13}$ - $10^{14} \text{g}$  PBHs, whose lifetime is shorter than the present age of the Universe ( $t_0 \approx \tau(5 \times 10^{14} \text{g})$ ), is expected to be concentrated at GeV band (the BH temperature  $T_{\text{BH}} \approx 1 \frac{10^{13} \text{g}}{M} \text{GeV}$  [3, 34]) in the co-moving reference frame, it would be redshifted to MeV band in the observed reference frame. Therefore, the HR from our considered PBHs should not significantly contribute to the IGRB above GeV. Secondly, since a considerable part of HR photons for energy  $\gtrsim 10 \text{GeV}$  propagating over cosmological distances would be absorbed by soft background (e.g., extragalactic background light) photons via electron-positron pair production, only low-redshift ( $z \lesssim 8$ ) PBHs could significantly contribute to the IGRB with corresponding energy.

Considerable efforts have been devoted to interpreting the IGRB in terms of a superposition of many unresolved extragalactic gamma-ray sources. It is widely believed that the observations between 100 to 200 keV are predominantly produced by coronal thermal emission from radio-quiet AGN (Seyferts) [37]. Recently, Ref. [26, 27] and [23] have explained the MeV (100 keV to several MeV) IGRB together with PeV neutrinos background as the accretion-disk emission in low-luminosity AGN. Meanwhile, other possible candidates including radio-loud AGN [22, 35, 36], Kilonovae and type-Ia supernovae, are found to only contribute a limited share to the MeV IGRB [51, 53]. We take into account the simulated IGRB of Kimura *et al* [27] into the analysis for PBH constraint, and the model from [23] is also discussed in Sec. V. The former seems more realistic [54, 55], where the thermal electrons inside hot accretion flows naturally emit soft gamma-rays via synchrotron self-Compton processes.

For the *100 MeV-5 GeV* IGRB, the primary candidate sources provided the bulk of such backgrounds are unresolved SFGs [25, 38–42] and radio galaxies (RG, misaligned radio-loud AGN) [43] (Blazar, aligned radio-loud AGN, should be the primary candidate at energy above  $\sim 5 \text{GeV}$  too [44, 45]). However, the contribution for SFG given by [43] has huge uncertainty from 10% to 100%, and a recent study of [21] finds that RGs only contribute 4%-18% of the IGRB using a large sample of Fermi-LAT RGs. The SFG origin for this IGRB is strongly favored by the recent work of [25], whose method is based on a physical model for the gamma-ray emission with no free parameters (all quantities that are measured directly) rather than simple empirical scalings. In addition, the statistical analyses of angular fluctuations in the IGRB and cross-correlations between IGRB and galaxies also support the SFG origin [41, 46]. Therefore, we model the astrophysical component in the IGRB below 5 GeV with the SFG contributions provided by [25].

The red dashed line in Fig. 3 represents the Roth *et al* model. The total flux from simulated “SFGs (Roth 2021)+AGNs (Kimura 2021)+PBHs” with  $M = 5 \times 10^{15}$  g and  $f = 8 \times 10^{-5}$  (black dash line) is represented by the red line. In this scheme, the IGRB round 10 MeV band still cannot be resolved, and thus we can expect that it gives a relatively weak constraint on the PBHs abundance in the relevant mass range.

#### IV. RESULTS: CONSTRAINTS ON THE PBH ABUNDANCE

In this section, we will present our results about the constraint on the PBH abundance  $f$  with monochromatic mass distribution in the interested mass range. Since angular momentum makes PBHs evaporate faster and thus makes the bounds on their abundance stronger, we assume a population of non-rotating PBHs in our simulation [5]. In this sense, our results are conservative compared to the case considering rotating PBHs.

##### A. Conservative constraint: without astrophysical component modeling

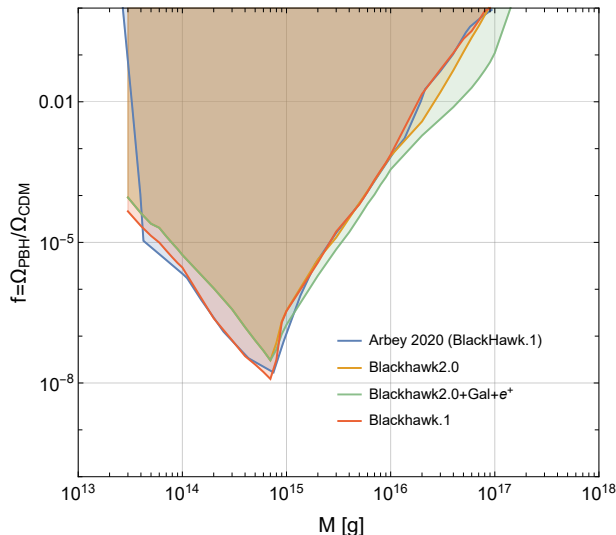


FIG. 4. 68% C.L. bounds derived without astrophysical background modeling. The green line represents the bound considered the direct Galactic PBHs HR and the radiation due to  $e^+$  annihilation, where the secondary spectra (and thus the whole HR flux) is reliably simulated with **BlackHawk.2.0** or Eq. (2). The orange line represents the bound without contribution from the Galactic PBHs and  $e^+$ , where the PBH flux is obtained with **BlackHawk.2.0** too. For comparison, we also show the constraint in the literature [4] by blue line and our bound (by red line) where we calculate the HR with the way of this literature.

We derive conservative bounds on the PBH abundance without above astrophysical component modeling. These

constraints require that the flux from PBHs, Eq. (3), does not exceed any measured IGRB data-points by more than  $1\sigma$ , as done in [5]. The bound thus obtained is displayed in Fig. 4 (green line), compared with that in the literature [4] (blue line). We rule out the totality of DM in the form of PBHs for  $10^{13}$  g  $\lesssim M \lesssim 10^{17}$  g with 68% C.L. The improvement over the upper limit given by [4] is significant, especially more than an order of magnitude improvement at  $2 \times 10^{16}$  g  $\lesssim M \lesssim 10^{17}$  g.

In order to distinguish where the improvement comes from, we also show the result (orange line) without the Galactic component of PBH HR and the indirect  $e^+$ -annihilation component in Fig. 4. As we can see, the improvement at  $3 \times 10^{13}$  g  $\lesssim M \lesssim 7 \times 10^{14}$  g results from the reliable calculation for the secondary spectra with **BlackHawk.2.0** or Eq. (2). As the photon flux calculated with Eq. (2) become stronger at relevant energy than that with **BlackHawk.1** (see the bottom panel in Fig. 1) for lighter PBHs, our constraint turns from more stringent to weaker at  $M \lesssim 7 \times 10^{14}$  g. At  $M \lesssim 10^{15}$  g, the additional component to the flux leads to the improvement. The reliable secondary-spectra calculation effects the improvement around  $3 \times 10^{16}$  g too.

We can repeat the bound of [4] well, which verifies our calculations, see the red line in Fig. 4.

##### B. With astrophysical component modeling

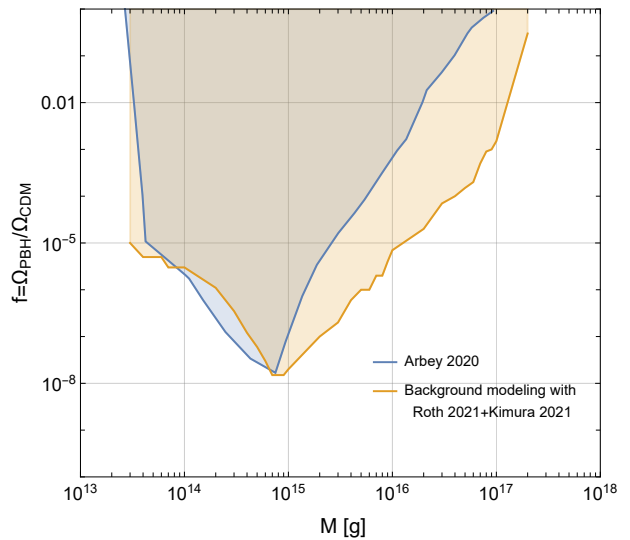


FIG. 5. Bound derived with astrophysical background modeling. The orange line represents the upper limit with 95% C.L. counting for the AGNs and SFGs contribution given by [27] and [25], respectively (see, Fig. 3). For comparison, we also show the constraint with 68% C.L. in the literature [4] by blue line.

Since the measured IGRB flux should contain the components from gamma-ray sources, such as AGNs and SFGs, more strength and realistic bounds on  $f$  would

be obtained if the components are accounted. Therefore, we add the astrophysical component given by [27] and [25] (see the “Kimura 2021” and “Roth 2021” lines in Fig. 3) into our simulated flux from the PBHs. Since the model [25] is beyond the upper limit of the data-points at several GeVs, the uncertainties in Galactic-foreground modeling are added in quadrature to the Fermi-LAT data<sup>3</sup> [48], and thus, our constraint is derived if the simulated flux does not exceed any measured IGRB data-points by more than  $2\sigma$ .

Fig. 5 shows our bound with orange line and that in [4] (with 68% C.L.) for comparison. Our improvements in simulating the diffuse flux, i.e., calculating the secondary spectra with `BlackHawk.2.0` and including the  $e^+$ -annihilation radiation, Galactic PBH component, and the astrophysical background, lead to more than an order of magnitude tighter constraint at  $10^{15} \text{ g} \lesssim M \lesssim 10^{17} \text{ g}$ , pushing the constrained PBH mass to  $M = 2 \times 10^{17} \text{ g}$ . Since the “Kimura+Roth” model can only account for a small fraction of the IGRB at 20-100 MeV where the HR emitted by PBHs of  $10^{14} \text{ g} \lesssim M \lesssim 10^{15} \text{ g}$  is concentrated, the improvement at this mass band due to the inclusion of the background is not significant.

## V. DISCUSSION

In this section, we will discuss other model explaining the measured IGRB.

The model in [23] can also explain the MeV background together with PeV neutrinos background with the accretion-disk emission in low-luminosity AGN. Based on the observation evidence of nonthermal synchrotron emission in two nearby Seyfert galaxies, the MeV gamma-rays are generated by nonthermal electrons via inverse Compton scattering of disk photons in this model, rather than thermal electrons via Comptonization of their synchrotron photons as in [27]. Fig. 6 (top) displays this model with blue dash line and the total of the three models (Inoue 2019 [23]+Roth 2021 [25]+PBHs) with maroon line.

The derived bound using the analysis method described in Sec. IV B is reported in the bottom panel of Fig. 6 by green line. Not surprisingly, the advance in the treatment of the simulated flux notably improves the constraint on  $f$  over that from [4] (blue line) at most of the considered mass range. The “Inoue 2019 + Roth 2021” bound is more conservative at high mass band  $10^{15} \text{ g} \lesssim M \lesssim 2 \times 10^{17} \text{ g}$  but more stringent below  $10^{15} \text{ g}$  than the “Kimura 2021 + Roth 2021” one (green line). These phenomena can be attributed to the relative size of the contributions of the two background models to the IGRB. Namely, the flux modeled by Kimura 2021 (blue

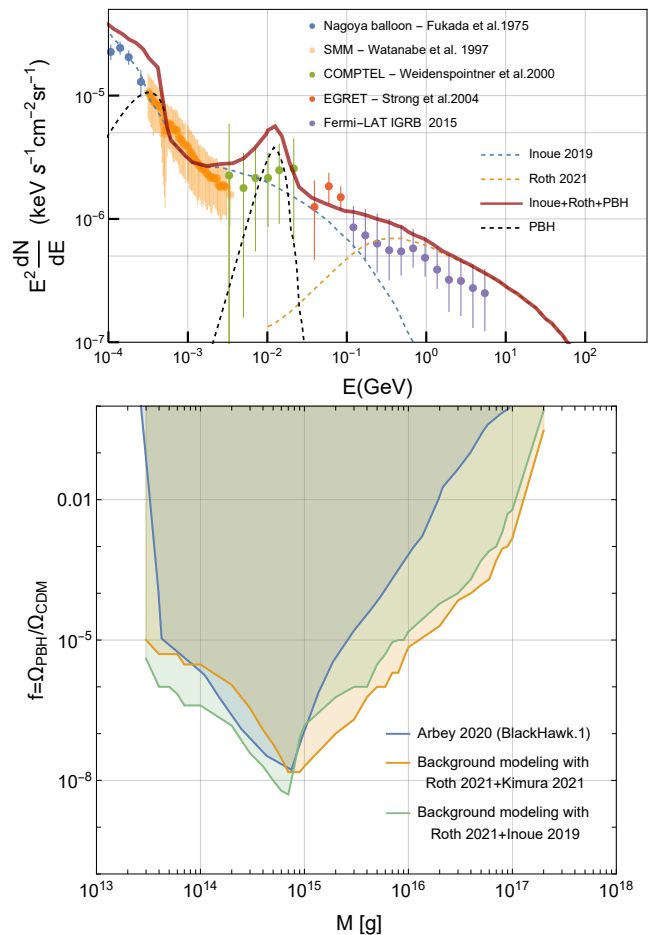


FIG. 6. Top panel: Same as Fig. 3, but the MeV astrophysical background is considered with the model in [23] (blue dashed line). The sum of models Inoue 2019 [23], Roth 2021 [25] and PBH is shown with maroon line. Bottom panel: bounds at 95% C.L. accounting for astrophysical background modeling. The green line represents the result of the AGNs and SFGs contribution given by [23] and [25], respectively. For comparison, we also show the constraint in the literature [4] by blue line and that for “Roth 2021+Kimura 2021” model in Fig. 5.

dashed line in the top panel of Fig. 3) above 2 MeV is more conservative than Inoue 2019 [23] but slightly higher at 100 keV-2 MeV. These results suggest that the Fermi-LAT observations only mainly affect the constraint on the PBHs around  $8 \times 10^{14} \text{ g}$ .

Future MeV space missions, such as GRAMS [56], AMEGO [57, 58], XGIS-THESEUS [59], and e-ASTROGAM [60], will be able to detect a larger number of point sources and will help to verify the models for the unresolved astrophysical background and thus test our constraints on the PBHs.

## VI. CONCLUSION

In this article, a population of PBHs with monochromatic mass distribution in the range  $10^{13} \text{ g} - 10^{18} \text{ g}$  has

<sup>3</sup> If the model is still beyond the upper limit of the data-points, the statistical uncertainty is expanded to several  $\sigma$  so that the model value is below the upper limit of the data.

been considered. New upper limits on the PBH abundance  $f$  constituting all or part of the DM have been set by comparing the measured IGRB flux at 100 keV–5 GeV band with the diffuse flux from the Galactic and extragalactic Hawking radiation.

We have reliably calculated the secondary spectra produced by primary particles for energy below 5 GeV according to Eq. (1), with the latest public code `BlackHawk.2.0` [28]. As a result, the conservative upper limit at  $3 \times 10^{13} \text{ g} \lesssim M \lesssim 7 \times 10^{14} \text{ g}$  is several times weaker than the relevant one of Arber *et al.* [4] but stronger at around  $3 \times 10^{16} \text{ g}$ , see Fig. 4. Furthermore, our model takes into account the Galactic PBHs’ diffuse radiation and that of the positronium annihilation from evaporated positrons, see Eq. (5) and (7). The resulting constraint on  $f$  is significantly improved over literature Arber *et al.* [4], especially more than an order of magnitude at  $2 \times 10^{16} \text{ g} \lesssim M \lesssim \times 10^{17} \text{ g}$ , see Fig. 4.

After further accounting for the astrophysical background model given by [26, 27] and [25], the constraint is tighter more than an order of magnitude at  $10^{15} \text{ g} \lesssim M \lesssim 10^{17} \text{ g}$  compared to [4], pushing the constrained

PBH mass to  $M = 2 \times 10^{17} \text{ g}$ , see Fig. 5.

Other constraints, based on the alternative astrophysical model [23] explaining the MeV IGRB, are also discussed (see Fig. 6). They are helpful to comprehend the uncertainties of our results from the astrophysical background modeling. For general extended mass function, the corresponding bounds should be tighter or similar (see e.g., [4, 6]). Future MeV telescopes are hoped to test our constraints with background modeling.

## ACKNOWLEDGMENTS

We thank Seishi Enomoto, Yi-Lei Tang, and Chengfeng Cai for useful discussions and comments. This work is supported by the National Natural Science Foundation of China (NSFC) under Grant No. 11875327, the Fundamental Research Funds for the Central Universities, China, and the Sun Yat-sen University Science Foundation.

- 
- [1] B. Carr and F. Kühnel, *Primordial Black Holes as Dark Matter: Recent Developments*, Annu. Rev. Nucl. Part. Sci. **70**, 355 (2020).
  - [2] M. Yu. Khlopov, *Primordial black holes*, Res. Astron. Astrophys. **10** 495 (2010)
  - [3] B. J. Carr, K. Kohri, Y. Sendouda and J. Yokoyama, *New cosmological constraints on primordial black holes*, Phys. Rev. D **81**, 104019 (2010)
  - [4] A. Arber, J. Auffinger and J. Silk, *Constraining primordial black hole masses with the isotropic gamma ray background*, Phys. Rev. D **101**, no.2, 023010 (2020)
  - [5] G. Ballesteros, J. Coronado-Blázquez and D. Gaggero, *X-ray and gamma-ray limits on the primordial black hole abundance from Hawking radiation*, Phys. Lett. B **808**, 135624 (2020)
  - [6] J. Iguaz, P. D. Serpico and T. Siebert, *Isotropic X-ray bound on Primordial Black Hole Dark Matter*, Phys. Rev. D **103**, no.10, 103025 (2021)
  - [7] J. Auffinger, *Limits on primordial black holes detectability with Isatis: A BlackHawk tool*, arXiv:2201.01265.
  - [8] B. Carr, K. Kohri, Y. Sendouda and J. Yokoyama, *Constraints on primordial black holes*, Rep. Prog. Phys. **84** 116902 (2021)
  - [9] A. Coogan, L. Morrison and S. Profumo, *Hazma: A Python Toolkit for Studying Indirect Detection of Sub-GeV Dark Matter*, Cosmol. Astropart. Phys **01**, 056 (2020).
  - [10] V. Poulin, J. Lesgourgues and P. D. Serpico, *Cosmological constraints on exotic injection of electromagnetic energy*, Cosmol. Astropart. Phys **03**, 043 (2017)
  - [11] P. Stecker, M. Krmer, J. Lesgourgues, and V. Poulin, *J. Exotic energy injection with ExoCLASS: application to the Higgs portal model and evaporating black holes*, Cosmol. Astropart. Phys. **03** (2018) 018.
  - [12] S. J. Clark, B. Dutta, Y. Gao, L. E. Strigari, and S. Watson, *Planck constraint on relic primordial black holes*, Phys. Rev. D **95**, 083006 (2017).
  - [13] M. Boudaud and M. Cirelli, *Voyager 1  $e^\pm$  Further Constrain Primordial Black Holes as Dark Matter*, Phys. Rev. Lett. **122**, 041104 (2019).
  - [14] W. DeRocco and P. W. Graham, *Constraining Primordial Black Hole Abundance with the Galactic 511 keV Line*, Phys. Rev. Lett. **123**, no.25, 251102 (2019).
  - [15] R. Laha, *Primordial Black Holes as a Dark Matter Candidate Are Severely Constrained by the Galactic Center 511 keV  $\gamma$ -Ray Line*, Phys. Rev. Lett. **123**, no.25, 251101 (2019).
  - [16] R. Laha, J. B. Muñoz and T. R. Slatyer, *INTEGRAL constraints on primordial black holes and particle dark matter*, Phys. Rev. D **101**, no.12, 123514 (2020).
  - [17] R. Laha, P. Lu and V. Takhistov, *Gas heating from spinning and non-spinning evaporating primordial black holes*, Phys. Lett. B **820**, 136459 (2021).
  - [18] B. Dasgupta, R. Laha and A. Ray, *Neutrino and positron constraints on spinning primordial black hole dark matter*, Phys. Rev. Lett. **125**, no.10, 101101 (2020).
  - [19] S. Wang, D. M. Xia, X. Zhang, S. Zhou and Z. Chang, *Constraining primordial black holes as dark matter at JUNO*, Phys. Rev. D **103**, no.4, 043010 (2021).
  - [20] A. Coogan, L. Morrison and S. Profumo, *Direct Detection of Hawking Radiation from Asteroid-Mass Primordial Black Holes*, Phys. Rev. Lett. **126**, no.17, 171101 (2021)
  - [21] F. W. Stecker, C. R. Shrader and M. A. Malkan, *The Extragalactic Gamma-Ray Background from Core Dominated Radio Galaxies*, Astrophys. J. **879**, no.2, 68 (2019)
  - [22] Y. Inoue, *Contribution of the Gamma-ray Loud Radio Galaxies Core Emissions to the Cosmic MeV and GeV Gamma-Ray Background Radiation*, Astrophys. J. **733**, 66 (2011)

- [23] Y. Inoue, D. Khangulyan, S. Inoue and A. Doi, *On high-energy particles in accretion disk coronae of supermassive black holes: implications for MeV gamma rays and high-energy neutrinos from AGN cores*, *Astrophys. J.* **880**, 40 (2019)
- [24] A. Arbey and J. Auffinger, *BlackHawk: A public code for calculating the Hawking evaporation spectra of any Black Hole distribution*, *Eur. Phys. J. C.* **79**, 693 (2019).
- [25] M. A. Roth, M. R. Krumholz, R. M. Crocker and S. Celli, *The diffuse  $\gamma$ -ray background is dominated by star-forming galaxies*, *Nature* **597**, no.7876, 341-344 (2021)
- [26] K. Murase, S. S. Kimura and P. Meszaros, *Hidden Cores of Active Galactic Nuclei as the Origin of Medium-Energy Neutrinos: Critical Tests with the MeV Gamma-Ray Connection*, *Phys. Rev. Lett.* **125**, no.1, 011101 (2020)
- [27] S. S. Kimura, K. Murase and P. Mészáros, *Soft gamma rays from low accreting supermassive black holes and connection to energetic neutrinos*, *Nature Commun.* **12**, 5615 (2021)
- [28] A. Arbey and J. Auffinger, *Physics Beyond the Standard Model with BlackHawk v2.0*, *Eur. Phys. J. C.* **81**, 10 (2021)
- [29] N. Aghanim *et al.* [Planck], *Planck 2018 results. VI. Cosmological parameters*, *Astron. Astrophys.* **641**, A6 (2020) [erratum: *Astron. Astrophys.* **652**, C4 (2021)]
- [30] N. Guessoum, P. Jean and W. Gillard, *The Lives and deaths of positrons in the interstellar medium*, *Astron. Astrophys.* **436**, 171 (2005)
- [31] N. Prantzos, C. Boehm, A. M. Bykov, R. Diehl, K. Ferriere, N. Guessoum, P. Jean, J. Knoedlseder, A. Marcowith and I. V. Moskalenko, *et al.* *The 511 keV emission from positron annihilation in the Galaxy*, *Rev. Mod. Phys.* **83**, 1001-1056 (2011)
- [32] R. J. Murphy, G. H. Share, J. G. Skibo, and B. Kozlovsky, *The Physics of Positron Annihilation in the Solar Atmosphere*, *Astrophys. J. S.* **161**, 495 (2005).
- [33] E.V. Karukes, M. Benito, F. Iocco, R. Trotta and A. Geringer-Sameth, *A robust estimate of the Milky Way mass from rotation curve data*, *J. Cosmol. Astropart. Phys.* **05** (2020) 033.
- [34] K. M. Belotsky, A. E. Dmitriev, E. A. Esipova, V. A. Gani, A. V. Grobov, M. Yu. Khlopov, A. A. Kirillov, S. G. Rubin and I. V. Svadkovsky, *signatures of primordial black hole dark matter*, *Mod. Phys. Lett. A*, **29**, 1440005 (2014)
- [35] K. Toda, Y. Fukazawa and Y. Inoue, *Cosmological Evolution of Flat-spectrum Radio Quasars Based on the Swift/BAT 105 Month Catalog and Their Contribution to the Cosmic MeV Gamma-Ray Background Radiation*, *Astrophys. J.* **896**, no.2, 172 (2020)
- [36] Ajello, M. and Shaw, M. S. and Romani, R. W. and Dermer, C. D. and Costamante, L. and King, O. G. and Max-Moerbeck, W. and Readhead, A. and Reimer, A. and Richards, J. L. and et al, *The Luminosity Function of Fermi-detected Flat-Spectrum Radio Quasars*, *Astrophys. J.* **751**, no.2, 108 (2012)
- [37] Y. Ueda, M. Akiyama, G. Hasinger, T. Miyaji and M. G. Watson, *Toward the Standard Population Synthesis Model of the X-Ray Background: Evolution of X-Ray Luminosity and Absorption Functions of Active Galactic Nuclei Including Compton-Thick Populations*, *Astrophys. J.* **786**, 104 (2014)
- [38] Fields, B. D. and Pavlidou, V. and Prodanovic, T, *Cosmic gamma-ray background from from star-forming galaxies*, *Astrophys. J.* **722**, no.2, L199 (2010)
- [39] Lacki, Brian C., Shunsaku Horiuchi, and John F. Beacom, *The star-forming galaxy contribution to the cosmic MeV and GeV gamma-ray background*, *Astrophys. J.* **786**, no.1, 40 (2014)
- [40] I. Tamborra, S. Ando and K. Murase, *Star-forming galaxies as the origin of diffuse high-energy backgrounds: Gamma-ray and neutrino connections, and implications for starburst history*, *J. Cosmol. Astropart. Phys.* **09**, 043 (2014)
- [41] J. Q. Xia, A. Cuoco, E. Branchini and M. Viel, *Tomography of the Fermi-lat  $\gamma$ -ray Diffuse Extragalactic Signal via Cross Correlations With Galaxy Catalogs*, *Astrophys. J. Suppl.* **217**, no.1, 15 (2015)
- [42] T. Linden, *Star-Forming Galaxies Significantly Contribute to the Isotropic Gamma-Ray Background*, *Phys. Rev. D* **96**, no.8, 083001 (2017)
- [43] M. Di Mauro, F. Calore, F. Donato, M. Ajello and L. Latronico, *Diffuse  $\gamma$ -ray emission from misaligned active galactic nuclei*, *Astrophys. J.* **780**, 161 (2014)
- [44] Y. Qu, H. Zeng and D. Yan, *Gamma-ray luminosity function of BL Lac objects and contribution to the extragalactic gamma-ray background*, *Mon. Not. Roy. Astron. Soc.* **490**, no.1, 758-765 (2019)
- [45] M. Di Mauro, F. Donato, G. Lamanna, D. A. Sanchez and P. D. Serpico, *Diffuse  $\gamma$ -ray emission from unresolved BL Lac objects*, *Astrophys. J.* **786**, 129 (2014)
- [46] S. Ando, M. Fornasa, N. Fornengo, M. Regis and H. S. Zechlin, *Astrophysical interpretation of the anisotropies in the unresolved gamma-ray background*, *Phys. Rev. D* **95**, no.12, 123006 (2017)
- [47] K. Watanabe<sup>1</sup>, D. H. Hartmann<sup>2</sup>, M. D. Leising<sup>2</sup>, L.-S. The<sup>2</sup>, G. H. Share<sup>3</sup>, and R. L. Kinzer<sup>3</sup> *The Cosmic Gamma-ray Background from supernovae*, *AIP Conference Proceedings*, AIP (1997)
- [48] M. Ackermann *et al.*, *The spectrum of isotropic diffuse gamma-ray emission between 100 MeV and 820 GeV*, *Astrophys. J.* **799**, 86 (2015)
- [49] Kappadath, S *et al.*, *The Preliminary Cosmic Diffuse gamma-Ray Spectrum from 800 keV to 30 MeV Measured with COMPTEL*, *Astronomy and Astrophysics Supplement Series.* **1356**, 120 (1995)
- [50] Hunter, S. D. *et al.*, *EGRET Observations of the Diffuse Gamma-Ray Emission from the Galactic Plane*, *Astrophys. J.* **481**, no.1, 205 (1997)
- [51] L. E. Strigari, J. F. Beacom, T. P. Walker and P. Zhang, *The Concordance Cosmic Star Formation Rate: Implications from and for the supernova neutrino and gamma ray backgrounds*, *J. Cosmol. Astropart. Phys.* **04**, 017 (2005)
- [52] Fukada, Y. *et al.*, *Rocket observation of energy spectrum of diffuse hard X-rays*, *Astrophysics and Space Science.* **32.1** (1975): L1-L5.
- [53] P. Ruiz-Lapuente, L. S. The, D. Hartmann, M. Ajello, R. Canal, F. K. Röpke, S. T. Ohlmann and W. Hillebrandt, *The origin of the cosmic gamma-ray background in the MeV range*, *Astrophys. J.* **820**, no.2, 142 (2016).
- [54] A. Kheirandish, K. Murase and S. S. Kimura, *High-energy Neutrinos from Magnetized Coronae of Active Galactic Nuclei and Prospects for Identification of Seyfert Galaxies and Quasars in Neutrino Telescopes*, *Astrophys. J.* **922**, no.1, 45 (2021)



- [55] E. M. Gutiérrez, F. L. Vieyro and G. E. Romero, *Non-thermal processes in hot accretion flows onto supermassive black holes: An inhomogeneous model*, *Astron. Astrophys.* **649**, A87 (2021)
- [56] T. Aramaki, P. O. H. Adrian, G. Karagiorgi, and H. Odaka, *Dual MeV gamma-ray and dark matter observatory-GRAMS Project*, *Astroparticle Physics.* **114**, 107 (2020).
- [57] J. McEnery *et al*, *All-sky Medium Energy Gamma-ray Observatory: Exploring the Extreme Multimessenger Universe*, *Bullet. Am. Astron. Soc.* **51**, 245 (2019).
- [58] A. Ray, R. Laha, J. B. Muñoz and R. Caputo, *Near future MeV telescopes can discover asteroid-mass primordial black hole dark matter*, *Phys. Rev. D* **104**, no.2, 023516 (2021).
- [59] D. Ghosh, D. Sachdeva, and P. Singh, *Future Constraints on Primordial Black Holes from XGIS-THESEUS*, arXiv:2110.03333.
- [60] A. De. Angelis *et al*, *The e-ASTROGAM mission. Exploring the extreme Universe with gamma rays in the MeV-GeV range*, *Exp. Astron.* **44**, 25 (2017).